Microelectrode miRNA Sensors Enabled by Enzymeless Electrochemical Signal Amplification

ARTICLE *in* ANALYTICAL CHEMISTRY · AUGUST 2015

Impact Factor: 5.64 · DOI: 10.1021/acs.analchem.5b00780 · Source: PubMed

4 AUTHORS, INCLUDING:

Emilie Viennois

Georgia State University

33 PUBLICATIONS **354** CITATIONS

SEE PROFILE

analytical chemistry

Article

pubs.acs.org/ac

Microelectrode miRNA Sensors Enabled by Enzymeless Electrochemical Signal Amplification

Tanyu Wang,[†,‡] Emilie Viennois,[‡,§] Didier Merlin,[*,‡,§] and Gangli Wang[*,†]

[†]Department of Chemistry, Georgia State University, Atlanta, Georgia 30302, United States

[‡]Institute for Biomedical Sciences, Center for Diagnostics and Therapeutics, Georgia State University, Atlanta, Georgia 30302, United States

[§]Atlanta Veterans Affairs Medical Center, Decatur, Georgia 30033, United States

Supporting Information

ABSTRACT: Better detections of circulating microRNAs (miRNAs) as disease biomarkers could advance diseases diagnosis and treatment. Current analysis methods or sensors for research and applications are challenged by the low concentrations and wide dynamic range (from aM to nM) of miRNAs in a physiological sample. Here, we report a one-step label-free electrochemical sensor comprising a triple-stem DNA-redox probe structure on a gold microelectrode. A new signal amplification mechanism without the need of a redox enzyme is introduced. The novel strategy overcomes the fundamental limitations of microelectrode DNA sensors that fail to generate detectable current, which is primarily due to the limited amount of redox probes in response to the target analyte binding. By employing a reductant, tris(2-carboxyethyl) phosphine hydrochloride (TCEP) in the detection buffer solution, each redox molecule on the detection probe is cyclically oxidized at the electrode and reduced by the reductant; thus, the signal is amplified in situ during the detection period. The combined merits in the diagnosis power of cyclic voltammetry and the high sensitivity of pulse voltammetry enable parallel analysis for method validation and optimization previously inaccessible. As such, the detection limit of miRNA-122 was 0.1 fM via direct readout, with a wide detection range from sub fM to nM. The detection time is within minutes, which is a significant improvement over other macroscopic sensors and other relevant techniques such as quantitative reverse transcription polymerase chain reaction (qRT-PCR). The high selectivity of the developed sensors is demonstrated by the discrimination against two most similar family sequences: miR-122-3p present in serum and 2-mismatch synthetic RNA sequence. Interference such as nonspecific adsorption, a common concern in sensor development, is reduced to a negligible amount by adopting a multistep surface modification strategy. Importantly, unlike qRT-PCR, the microelectrochemical sensor offers direct absolute quantitative readout that is amenable to clinical and in-home point-of-care (POC) applications. The sensor design is flexible, capable of being tailored for detection of different miRNAs of interest. Combined with the fact that the sensor was constructed at microscale, the method can be generalized for high throughput detection of miRNA signatures as disease biomarkers.

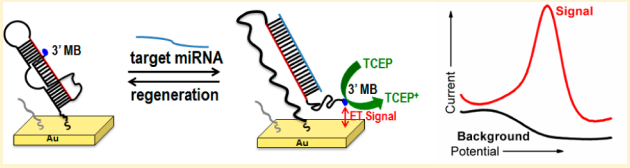

MicroRNAs (miRNAs) are a class of single-strand, short, endogenous nonprotein-coding RNAs with approximately 19−23 nucleotides.[1] In recent years, increasing evidence has indicated that miRNAs play important roles in a wide range of physiological processes, and their aberrant expressions are associated with various diseases.[2−4] Unlike most RNAs that are prone to degradation, recent reports suggest that a stable population of miRNAs exist in circulation.[5] Therefore, miRNA expression and quantitative profiles can be employed as biomarkers for the onset and progression of disease states.[6,7] However, the detection of miRNAs faces major challenges due to their unique characteristics, including low abundance and sequence similarity among family members.[8−11]

Capable methods or sensors featuring fast, low-cost detection with suitable sensitivity and selectivity for broad applications remain to be established.[1,12] Quantitative reverse transcription polymerase chain reaction (qRT-PCR) and microarray are the mainstream techniques for identification and quantitation of circulating miRNAs in plasma or serum.[13−15] Although microarray is a high throughput analysis platform, the sensitivity is not suitable for low-level miRNA quantitation.[14,16] The qRT-PCR is almost the unanimous choice for quantifying miRNAs due to its high sensitivity, but the methodology suffers from a time-consuming multistep analysis process and the requirement of highly-skilled personnel and a lab environment.[17−20] Moreover, most qRT-PCR analysis determines relative miRNA abundance (with respect to an often-not-validated reference miRNA) in biological samples which makes quantitative, point-of-care miRNA analysis not possible. Thus, there are urgent needs to directly obtain absolute concentration or quantity. Further, the complicated procedures and high-cost also prevent its applications in clinical and in-home point-of-

Received: February 26, 2015
Accepted: July 22, 2015
Published: August 4, 2015

DOI: 10.1021/acs.analchem.5b00780
Anal. Chem. 2015, 87, 8173−8180

Table 1. Triple-Stem DNA Probe (Recognition Sequence Marked in Blue) and Single-Stranded RNA Sequences (Mismatches Marked in Red) Used in the Microclectrochemical DNA-Sensor

Sequence name	(Abbreviation)	Sequence, listed 5' to 3'
Triple-stem DNA probe	(DNA)	/C6 SS/ GGA GTG TTT TTT TTC GTG TTT GTT TTT TCA AAC ACC ATT GTC ACA CTC CAT TTT TTT TTT TTG ACA ATG /MB/
mmu-miR-122	(miR-122)	UGG AGU GUG ACA AUG GUG UUU G
mmu-miR-122-3p	(miR-122-3p)	AGU GUG AUA AUG GCG UUU
2mismatch-22Base	(miR 22B)	UGG AGU GUG AUA AUG GCG UUU G

care (POC) applications. For more efficient detection of miRNAs with high sensitivity and selectivity, electrochemical sensors, among many others, have been developed to complement current methods and provide additional information as parallel analysis.[21−27] Particularly, the employment of DNA-/aptamer-based recognition coupled with electrochemical detection has become a popular method to develop rapid and quantitative folding-based sensors.[25−30] Further improvements in those promising sensors are needed to establish them as alternative methods complimenting or replacing qRT-PCR analysis.

The incorporation of micro- and nanoelectrodes in sensor fabrication has further pushed electrochemical sensing into new space and time domains recently.[31,32] The miniaturized detection platform is meritous for analysis of samples with limited quantity/volume at high throughput. A small-scale electrode offers unique properties such as high mass-transfer rate, small RC constants, and faster electrochemical responses.[31,33,34] With these improvements, miniaturized DNA-/aptamer-based sensors, specifically for the detection of DNAs and diagnostic proteins, attract substantial attention, but their implementation in miRNA detection is rare.[35] This is in part due to the key limiation of small sensor surface area when facing low abundance analytes, in which signal amplification is needed. We for the first time report the use of microscale electrochemical DNA sensors in the detection of miRNA-122 as a model system. The miRNA-122 is a unique sequence that is expressed in liver and conserved in vertebrates.[36] A down-regulation is linked to hepatocellular carcinoma (HCC) and an up-regulation is related to gastrointestinal disorders.[37,38] A self-hybridized, three-stem loop structure DNA sequence is designed following a previous report by Plaxco and co-workers as recognition probe.[39] The DNA probe is composed of a complementary sequence to the target miR-122 and a redox current reporter, methylene blue (MB), that functions as a signal-on one-step sensing mechanism. To overcome the limitation of low current associated with a small effective sensor surface, we introduce a chemical reaction mechanism following electron transfer reaction,[40] using a reductant tris(2-carboxyethyl) phosphine hydrochloride (TCEP) in the detection solution that will reduce the oxidized MB in situ at the detection electrical potential.[27] In this way, each MB molecule near the electrode surface, a consequence of recognizing a target miRNA molecule, will be cyclically oxidized electrochemically and reduced chemically by the reductant, a process that amplifies the signal.[41−43] Moreover, with a multistep surface modification procedure, the interference signal caused by nonspecific adsorption and surface bound redox signal probe is reduced to a negligible level, which has been a well-known technical barrier for sensor development. Improvements of this electrochemical analysis over qRT-PCR include one-step, rapid detection, direct quantification of absolute miRNA molecules, reduced cost, and user-friendly operation. Compared to other sensor-type detections, the signal amplification and background reduction here enable reproducible and reusable sensors for quantitative and one-step miRNA detection at an extremely low level within 10 min.

EXPERIMENTAL SECTION

Reagents and Materials. All solutions were prepared with RNase/DNase-free, ultrapure distilled water (Invitrogen). The following reagents were used as received: phosphate buffered saline (pH 7.4, 10×) (Life Technologies), magnesium chloride hexahydrate (99−102%, Sigma-Aldrich), guanidine hydrochloride (≥99%, Sigma-Aldrich), tris(2-carboxyethyl) phosphine hydrochloride (TCEP) (≥98%, Sigma-Aldrich), and 6-mercapto-1-hexanol (97%, Sigma-Aldrich). Thiolated, methylene blue-conjugated DNA (thio-MB-DNA) and micro RNAs (miR) were purchased from Biosearch Technologies (Novato, CA), purified by RP-HPLC. Sequences of DNA probe and single-stranded miRNAs used in this work are given in Table 1.

Preparation of the Electrode and DNA Monolayer Assembly. Gold microelectrode fabrication was carried out using a well-established method in our laboratory. Briefly, a 50 μm-diameter gold wire was attached to a tugsten rod using conductive silver epoxy. The gold−tungsten assembly was then inserted into a soda lime glass capillary, and then, the gold wire was sealed into the capillary using a natural gas-oxygen flame. The other end of the assembly was secured with a resin epoxy. Finally, the excess insulating glass is removed through manual polishing on sand paper (from rough to fine grit) to expose a gold wire resulting in a microdisk electrode with a 50 μm diameter. The gold electrode was polished carefully to a mirror surface on a 1200-grit sand paper followed by an aqueous slurry of 0.05 μm diameter alumina particles and then successively washed in an ultrasonic cleaner with water to remove excess polishing particles. Finally, the gold electrode was electrochemically polished by scanning the potential from −0.5 to +1.5 V in 0.1 M H_2SO_4 at a scan rate of 0.1 V s^{-1} for 10 cycles. The cleaned gold electrode was thoroughly washed with D.I. water and ethanol and dried under flowing nitrogen.

Prior to surface modification, 1 μL of 200 μM thiol-MB-DNA was mixed with 2 μL of 25 mM TCEP in a 200 μL PCR tube. The tube was incubated for 20 min at room temperature (21 °C) for reduction of disulfide bonds and to reduce the MB-moiety of the DNA probe. The solution was then diluted to a total volume of 200 μL in a high salt buffer (10 mM potassium phosphate, 30 mM sodium phosphate, 1.55 M sodium chloride, and 1 mM magnisium chloride, pH 7.2) to a final concentration of 1 μM. For immobilization, the previously cleaned gold electrode was transferred directly to the diluted and reduced thiol-MB-DNA solution and incubated for 16 h at room temperature in the dark. Following the formation of a self-assembled monolayer (SAM), excess thiol-MB-DNA physically adsorbed on the electrode surface was removed via a room temperature-deionized water rinse (~30 s). The DNA-probe-modified electrode was then immersed into 1 mM

DOI: 10.1021/acs.analchem.5b00780
Anal. Chem. 2015, 87, 8173−8180

mercaptohexanol in high salt buffer for 2 h. Next, the surface passivated microelectrode sensor was placed in a hybridization buffer (0.25 mM potassium phosphate, 0.75 mM sodium phosphate, 39 mM sodium chloride, and 10 mM magnesium chloride, pH 7.1). This solution was soaked in a water bath at 75 °C for 10 min. After the hybridization buffer cooled down to room temperature gradually in air, the microelectrode sensor was incubated with 1 mM meraptohexanol in high salt buffer for 1 h again for further surface passivation. Unless otherwise noted, all solutions used in the experiments to follow were carried out in hybridization buffer at pH 7.1. For convenient surface regeneration, hybridized sensors were rinsed in 4 M GHCl for 30 s followed by a 3 h incubation in hybridization buffer.

Electrochemical Measurements. Electrochemical measurements were performed using a Gamry Reference 600 electrochemistry workstation (Gamry Instruments, Warminster, PA) with a Ag/AgCl(s)/KCl(sat) reference electrode (Bioanalytical Systems, Inc.) and a gold working electrode. All potentials are reported relative to the saturated Ag/AgCl reference electrode. Electrochemical measurements were performed in hybridization buffer using cyclic voltammetry (CV) from −0.6 to +0.2 V or square wave voltammetry (SWV) with a 50 mV amplitude signal, over the range from −0.6 to +0.1 V versus Ag/AgCl reference. The oxidative peak of MB was detected by CV or SWV at −200 mV (vs Ag/AgCl) at the 10 min time point. MB was chosen as the redox tag due to its excellent shelf life and robust electrochemical response in serum compared to other redox tags, such as ferrocene.[44,45] The SWV response of each sensor was quantified as follows: (1) background (without target) and signal (with target) SWV data sets were collected; (2) difference traces were generated by subtraction of the two data sets; (3) baseline was corrected with B-spline generated baseline in Origin 8 using two regions: −0.60 to −0.40 V and −0.08 to +0.10 V; (4) traces were integrated from −0.40 to −0.08 V. To prepare calibration graphs, we report the average and deviations of two measurements on two different sensors for relatively high miR-122 concentrations from 10 fM to 0.5 nM, while for the low miR-122 concentrations of 0.1 and 1 fM the average of three measurements on two different sensors is reported. Selectivity tests with mismatched sequences were made in the same manner by substituting miR-122-3p or miR 22B for miR-122. Prior to the measurement of colitis mouse serum, a serum aliquot of 2 μL was heated for 15 min at 95 °C, followed by centrifugation to collect the sample. Then, the serum aliquot was diluted in 20 μL of buffer solution for easy handling and to make the current signal comparable with calibration measurements at the time for detection. The sensor was incubated for 10 min at room temperature prior to data collection.

RESULTS AND DISCUSSION

The principle of signal generation is illustrated in Scheme 1. The Au-disk microelectrode was prepared via a benchtop method that is routinely used in our lab for nanoelectrode fabrication. The radius r is typically 25 μm, characterized with 1 mM ferrocene (Figure S1).[46−48] The signal-on mechanism upon the recognition with target miRNAs is designed following the electrochemical DNA sensor strategy pioneered by Plaxco's group.[39] A nucleotide probe is designed to have multiple segments including a sequence perfectly complementary to miRNA-122 as target, an alkanethiol moiety at the 5′ terminus for self-assembly onto the gold surface, and a MB moiety at the 3′ terminus as redox signal reporter. The sequence of miR-122, designed probe, and two mismatches are listed in Table 1. To design new probes for different miRNAs, the binding sequence portion can be conveniently replaced, with the other portions adjusted accordingly. In the absence of the target miRNA, the probe will self-hybridize into three distinct, short-base-pair stems that form a discontinuous double helix (left). With inert alkanethiolates passivating the remaining surface unoccupied by the DNA probes, the discontinuous double helix will lock the redox molecule, MB, away from the electrode, and thus largely shut down electron transfer pathways. Signal is turned on only upon the recognition with the target miRNA. The probe−target hybridization is energetically favored by the formation of longer double strand over the disruption of the discontinuous triple-stem structure. The process liberates a flexible segment near the MB-labeled 3′ terminus, which in turn enables the electron transfer (ET) reaction of the redox MB with the electrode and generates the faradaic ET current that is a function of the accessible miRNAs (right).

Scheme 1. Current Amplification in the Signal-on Microelectrode Sensor[a]

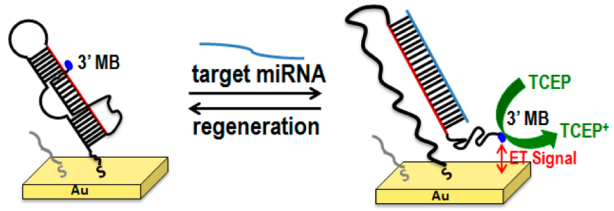

[a]Reduction by TCEP in the solution of the electrode-oxidized MB on the surface amplifies the current signal. Inert OH terminated alkane (C6) thiols are used to passivate the electrode surface as spacers to support the probe on the surface.

A crucial multistep surface modification strategy is developed to optimize the sensor surface such that background ET current is negligible. In most electrochemical sensors to date, nonspecific adsorption on sensor surfaces is detrimental for applications because it induces interference signals that limit the quantification, particularly for low abundance analytes. As shown in Figure S2, the MB oxidation peak at −200 mV indicates a nonideal surface after the commonly adopted one-step modification. It is rather common to have nonideal surface packing with defect sites, often referred as pin holes in self-assembled monolayers. The redox probes could lean down and interact with the electrode for ET after the first passivation step, generating target-independent background current. To improve the quality of the passivating monolayer and suppress background current, we applied a heating/cooling cycle, a procedure that allows rearrangement of the thiolates on the Au surface detailed in the Experimental Section. After a second passivation step with the same inert thiols, baseline-level nonfaradic charging current, indicating almost ideal surface modification, was achieved in both cyclic voltammetry (CV) and square wave voltammetry (SWV) measurements (blue curves in Figure 1). This observation indicates that those defect sites, i.e., pinholes in the thiolate layer, are further filled by the alkanethiolates after the second passivation step. The high quality surface functionalization therefore makes the sensor highly resistant to common interferences such as nonspecific adsorptions, also including oxygen molecule permeation and the collapse of MB-DNA probes.

DOI: 10.1021/acs.analchem.5b00780
Anal. Chem. 2015, 87, 8173−8180

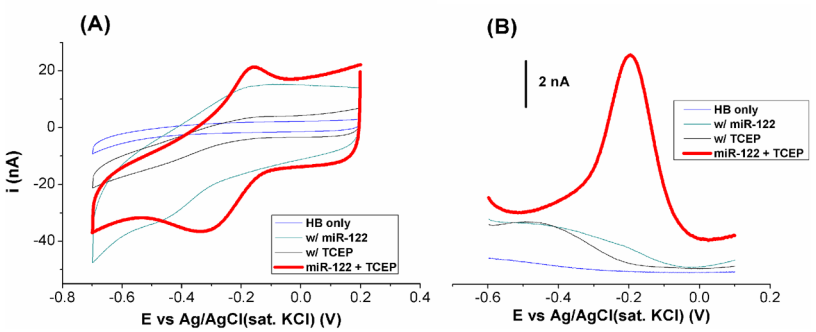

Figure 1. Microelectrode miRNA sensor with TCEP amplification in hybridization buffer (HB), pH 7.1. (A) Cyclic voltammograms (CVs) recorded at a scan rate of 5 V s^{-1}. Clean background was obtained in buffer only (blue). The successful suppression of O_2 reduction indicates good sensor surface coverage after a two-step passivation procedure. Addition of 160 μM TCEP or 0.5 nM miR-122 in HB results in the increase of charging current with irresolvable anodic current (black or green). Addition of both TCEP and miR-122 exhibits greatly improved oxidative signal (red). (B) Corresponding anodic square wave voltammograms (SWVs) of the DNA-senor. Data were recorded at a frequency of 100 Hz.

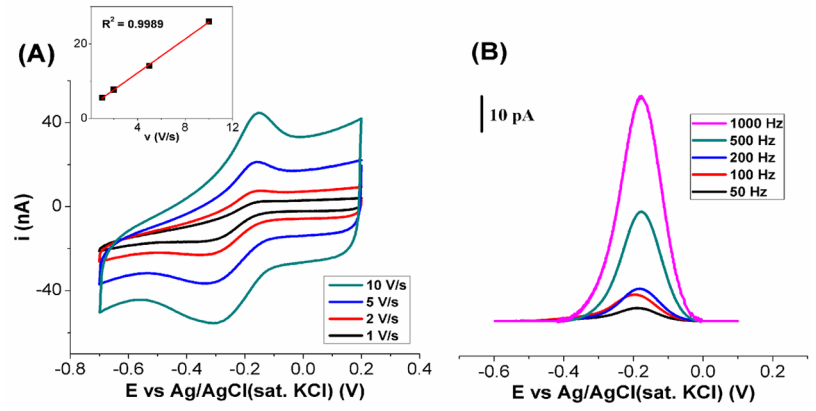

Figure 2. Differentiation of the faradic ET current induced by target-binding from the capacitive background current. Data recorded in 0.5 nM miR-122 and in the presence of 160 μM TCEP. (A) CVs at different scan rates. The inset shows a linear correlation between the anodic peak current and scan rate. (B) SWVs at different frequencies (scan rates). Baseline was adjusted to better display the trend. Original data are included in Figure S4.

A major limitation associated with surface-based electrochemical sensors is that the signal intensity depends on the surface coverage of probes. Once a MB molecule is oxidized at a given potential, it loses ET activity to generate the detection signal until reactivated via reduction. To enhance the sensitivity, we introduce a chemical reagent (reductant) in bulk solution that reduces the oxidized MB in situ at the detection potential. As shown in Figure 1, well-resolved anodic current can be observed only in the presence of both TCEP and miR-122, in both CV and SWV measurements (red curves). Only anodic peak currents were studied in this work due to the presence of the oxygen reduction peak that overlaps partially with that of MB at ca. −0.3 to −0.4 V. As controls, negligible anodic currents were detected in CV in the presence of TCEP but without miR-122, suggesting that TCEP will not interfere with measurements within the detection potential window of MB (black curves). CV responses at different TCEP concentrations are included in Figure S3. A slight distortion in baseline at around −0.4 V is consistently observed after the addition of TCEP, particularly in SWV. The distorted baseline measured prior to the addition of target is used as background current and subtracted from the signal current in the quantitative analysis. The miRNA-122 itself without TCEP causes a slight increase in anodic current in both CV and SWV that is barely discernible from baseline current. This low signal level constitutes a common problem for miniaturized electrodes and sensors (green curves) in general. The parallel current traces in CV arise from simple capacitive charging and discharging of the double layer that does not interfere with the data analysis elaborated in the later sections.

The key to the signal amplification is the reductive property of TCEP. In the detection system, each MB molecule near the electrode surface, a consequence of recognizing a target miRNA molecule, will be cyclically oxidized at the electrode and reduced by the reductant, thus greatly amplifying the signal during the detection period. In analogy, the surface-bound probes can be considered to function as the Gate (with each MB as a "tunnel") while the reductant in solution and the electrode were the Source and Drain in electron tunneling or field-effect transistors, respectively. Many efforts have been put into the development of electrocatalytic strategies for DNA sensors.[41−43] To the best of our knowledge, direct detection of ET current in CV has not been achieved in folding-based DNA electrochemical sensing literature, especially with microelectrodes. Pulsed techniques such as SWV or differential pulse voltammetry (DPV) were necessary to resolve the ET signals, which involves complex kinetics and could generate false positive or false negative responses at different measurement conditions. Nonspecific physical/mechanical interactions could cause the DNA probe to collapse or deform and cause electron transfer between the collapsed DNA-MB and electrode surface, which induce false positive signals.[25−27] False negative has been

DOI: 10.1021/acs.analchem.5b00780
Anal. Chem. 2015, 87, 8173−8180

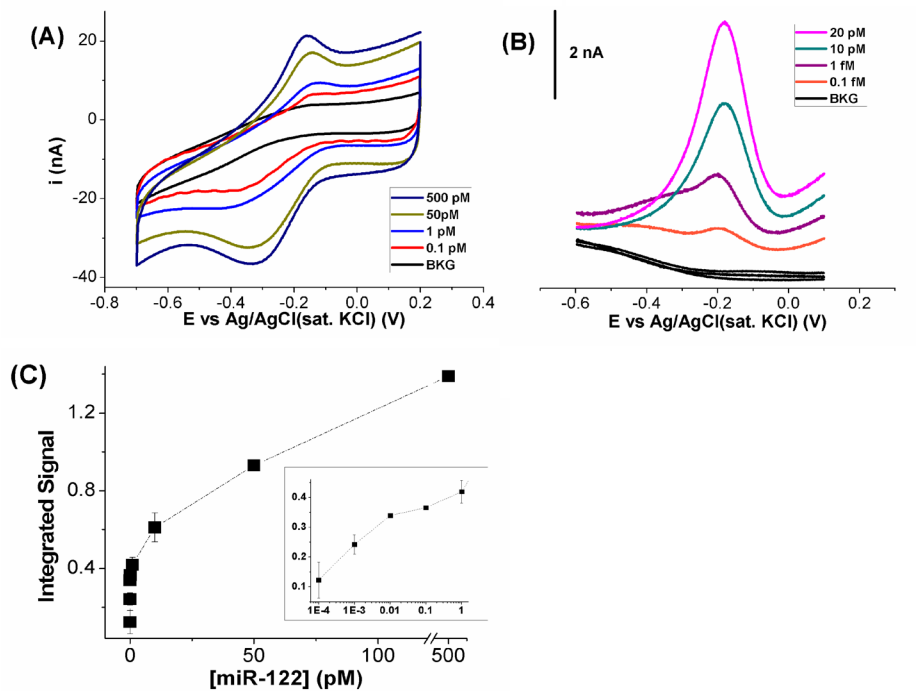

Figure 3. Sensor responses at different miR-122 concentrations. (A) CVs and (B) SWVs at representative concentrations. CV data were recorded at a scan rate of 5 V s^{-1} at 10 min after the addition of target. SWV frequency is 100 Hz. The sensor was regenerated (overlapping black curves in (B) as background demonstrating the excellent sensor recovery) following each measurement by a simple wash with 4 M guanidine chloride (GHCl). (C) A quantitative correlation between the integrated signal in SWV and miR-122 concentration over a wide range from 0.1 fM to 0.5 nM. The inset shows the trend at the lower concentration range in log plot. All data represents the average and standard deviation of two sensors. Full SWV data and analysis are included in the Supporting Information. The error bar on some points are too small to be seen visually. A dashed line was added to illustrate the trend (not fitting).

reported at extremely high frequencies, especially in the case of a target-saturated surface.[49] Data from both CV and SWV will better reveal the signal generation mechanism and thus enable better method design and development. Besides the signal amplification mechanism, we discovered that detection current can reach a measurable level at each concentration within 10 min, which is substainitially faster compared to its counterpart fabricated on macroscale gold electrodes that require a 3 h incubation prior to each measurement in previous reports.[39] The fast detection is achieved benefiting from the greatly enhanced mass transport kinetics at microelectrodes.

The faradic ET current signal resulting from the target binding can be quantified and differentiated from background current such as capacitive charging−discharging at the sensor surface under optimized measurement conditions. The observed CV features at different scan rates are characteristic for electrodes at the transition size range between macro-electrodes and ultramicro/nanoelectrodes. At relatively low scan rates (1 V/s or lower), the anodic current in CVs (Figure 2A) shows a plateau that is characteristic of diffusion limited microelectrode behavior. Note this diffusion process corresponds to the TCEP from bulk to the sensor surface because MB is immobilized on the microelectrode. At faster scan rates (5 and 10 V/s), mass transport rate is no longer sufficient relative to ET kinetics; thus, depletion near the electrode surface causes the anodic current to decrease at higher overpotentials. Accordingly, the CV features transform from micro- to macroelectrode-like behaviors. The shape transitions of CVs at different scan rates correspond to the TCEP diffusion behavior by considering each methylene blue tunneling the electron transfer as an individual nanoelectrode: the plateau current corresponds to the radial diffusion of TCEP, while faster ET kinetics at high scan rate induces depletion peak shape (i.e., $t^{1/2}$ decay). A linear correlation was established between anodic peak current and scan rate rather than square root of scan rate. The linear dependence reflects the radial diffusion at microelectrode and should not be confused as adsorption on macroelectrodes. It is important to mention that the current signal is enabled through surface-bound MB on the electrode. Baseline adjusted SWVs at varied frequencies further affirm the analysis (Figure 2B, original data was shown in Figure S4). Because capacitive charging current is largely subtracted in SWVs, the current peak is better resolved. The peak current displays a linear relationship with frequency within the range tested. At higher frequencies, the peak current decreases (results not shown) which is consistent with earlier reports that SWV peak current could decrease at higher frequency ranges at the DNA sensors.[49] The frequency of 100 Hz was used in later measurements considering the less distorted baseline and the uncertainty of charging current in varying solution conditions as well as possible impacts by different kinetic processes in signal generation at higher frequency.

The microelectrode sensor was further challenged for the quantification of miR-122 in phosphate buffer solution at pH 7.1. As shown in Figure 3A, baseline-level anodic current was obtained in the presence of only TCEP in buffer solution for up to 160 μM as background (BKG). Upon each addition of miRNA-122 at the denoted concentration, the methylene blue peak current in CVs measured after a 10 min-incubation increased. The corresponding SWVs show drastic improvements in resolving signals from background at low miRNA-122

DOI: 10.1021/acs.analchem.5b00780
Anal. Chem. 2015, 87, 8173−8180

levels below 0.1 pM for quantitation (Figures 3B and S5). However, it is known that the signal deliberated by SWV is highly dependent on the measurement parameters, such as the frequency, due to its sensitive nature to electrode reaction rates.[49] Figure S6 provides SWV data and peak analysis at a frequency of 1 kHz for comparison. The CVs, on the other hand, are better suited as diagnostic tools for method development. Previous studies could not take advantage of CVs because the current signal is generally too low to be detected. Both CV and SWVs were recorded at the mean time for parallel analysis and method validation. A large dynamic range (sub fM to nM) is established that could be further extended if necessary by the optimization in sensor design and measurement parameters.

Remarkably, the background current can be recovered repeatedly after each target miRNA measurement (bundled black curves in panel B of Figure 3). The finding demonstrates superb sensor stability and consistency that are vital for quantification and method development and optimization. A wide range of miR-122 concentrations from 0.1 fM to 500 pM was tested with two separate sensors. Although variations due to the differences in surface area and probe coverage were observed, current signals resulting from the same miR-122 concentration on different sensors remain comparable. Impressively, a detection limit of 0.1 fM was achieved that corresponds to 0.2 attomole of miR-122 molecules being detected. While we have not attempted to limit the detection volume used in establishing the calibration curve, a 20 μL sample is sufficient for this microelectrode-based sensor, corresponding to the detection of 1200 copies of miR-122 molecules within 10 min. The sensor performance in reduced analysis volume of 20 μL is demonstrated in the detection of mouse serum sample described later in this report. The capability is already approaching that of qRT-PCR but offers absolute quantification at drastically reduced time and cost. It is obvious that the low detection limit of our sensors could be further improved, which will be discussed in a later report that involves complex kinetics beyond the scope of this paper.

A Langmuir isotherm type curve was observed by plotting the integrated current signal from SWV as a function of miRNA-122 concentration as the calibration curve (Figure 3C). Because the current peak shape is conserved, integrated peak area is proportional to peak current in SWV results herein. Integrated current offers merits over a single point analysis (peak current) by ensemble averaging and thus reduces possible interferences such as random noise or baseline fluctuation. The trend is the direct consequence of the governing mechanism of signal generation. The detected current results from a series of kinetic processes including mass transport of miR-122 from solution to the surface, hybridization with surface DNA sequence, ET among the TCEP, MB, and the electrode, and the diffusion of TCEP. For simplicity in establishing the signal amplification concept in this report, the data in Figure 3C were collected at a fixed time (10 min incubation). For a given surface area (i.e., 25 μm radius) over a given period (10 min), the sensor surface would be saturated at high concentrations (i.e., the last point in Figure 3C), and thus, the current signal approaches a plateau; while at low concentrations, a qualitatively linear correlation with logarithm analyte concentration was detected as commonly observed for these types of sensors. In other words, a broad detection range over 6 orders of magnitude is established governed by different kinetic processes. Optimization of the detection parameters and the governing kinetics for mechanistic understanding are underway, which is expected to further broaden the detection range. Better linearity, with either concenration or logarithm concentration, will also be established at different time/concentration domains in which the rate limiting step is dominated by a single kinetic process.

It is important for method validation and quantitative analysis that the sensor can be conveniently regenerated, although it might not be critical for practical applications. The negligible baseline-level background current can be regenerated after a 30 s room temperature wash with 4 M GHCl followed by a 3 h incubation in buffer solution repeatedly (Figure S7). GHCl is known to disrupt hydrogen bonds in double stranded DNAs and thus help release target miRNAs from surface bond DNA probes. Upon incubation in HB, the thermodynamically stable triple-stem structure is restored at room temperature within 3 h. Accordingly, the sensor response can be regenerated with a mean recovery of near 100% of the initial signal (Figure 4). A gradual rise of background current and decline of signal

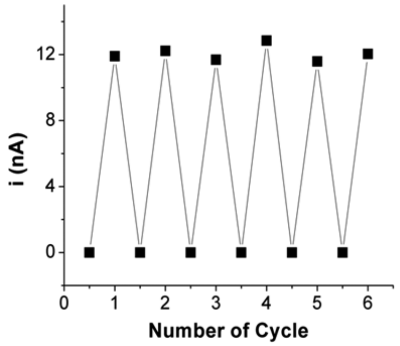

Figure 4. Regeneration and stability of the microelectrode-based electrochemical DNA-sensors. Reproducible results were achieved with GHCl wash in the detection of 50 pM miRNA-122. Sensors can be readily regenerated for at least 6 times without any loss of sensitivity. Additionally, sensors can be stable after a 2-month storage in dry-form at room temperature. Current was obtained from CV measurements after charging current subtraction.

current become noticeable after more than six cycles for this sensor. The deterioration is attributed to the degradation of the thiolate SAMs that is known for the analysis in biological media.[40] If resuable sensor is needed, the stability could be further improved by the optimization of SAM including using longer carbon chains for the inert spacer and employing multidentate thiols, etc.[50] More excitingly, the sensor was found to preserve its function after a two-month storage in dry form (data not shown). The superb stability is credited to the chemical stability of the DNA probe, the covalent attachment to the electrode surface, and the optimized multistep surface modification.

The sensor specificity was evaluated with two physiological analogs: a two-base mismatched miR-122-3p with 18 bases and a synthetic two-base mismatched miR 22B of 22 bases that has the same length as the target miR-122. Essentially, no response was observed in the presence of 200 pM miR-122-3p or miR 22B even after a 30 min incubation. To affirm the efficacy of the exact sensor, with a 10-fold lower miR-122 (20 pM), the signal raised substantially in 10 min (Figure S8). The superior discriminiation against mismatched bases at room temperature results from the distinct thermodynamic properties in the triple-stem structure independent of the electrochemistry signal

DOI: 10.1021/acs.analchem.5b00780
Anal. Chem. 2015, 87, 8173−8180

amplification mechanism described in this report. The location of the mismatches in the physiological analogs, i.e., in the middle of the sequences or toward the end, and the identity of the mismatched bases as well as the length of the nonspecific sequences are factors to consider in the design of probes for other miRNA sequences.

To illustrate the efficacy of the sensor in complicated matrix and mimic the detection in real point-of-care settings, serum sample from a colitic mouse was tested. As shown in Figure 5,

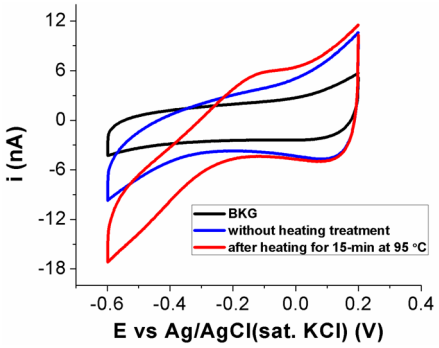

Figure 5. Sensor responses to colitis mouse serum sample. Data was collected at the 10 min time point to be consistent with earlier measurements.

the expected anodic current from the cyclical oxidation of MB and reduction by TCEP upon binding with target miRNAs was observed at 10 min in a diluted serum sample. The results suggest that the signal generation mechanism remain effective in the complex physiological matrix. It is worth mentioning that a heating treatment of the serum sample is required. This is because the microRNAs are either stabilized by proteins or encapsulated in vesicles in serum/blood. Therefore, the curve (without heating) illustrates the resistance of the sensor detection mechanism to the complicated matrix including nonspecific adsorption of proteins and lipids in physiological samples. More quantitative analysis of miRNAs in physiological samples requires further optimization of measurement conditions and better understanding of different kinetic processes that will be discussed in a future report.

CONCLUSIONS

Electrochemical signal amplification is employed in the development of the microelectrode sensors for one-step detection of miRNAs within 10 min. We used a common reductant, TCEP, and a target sequence, miR-122, as the model system to demonstrate the sensor efficacy evaluated by potential sweeping CV and pulsed SWV techniques. Benefitting from the multistep surface modification method, background current was minimized to the baseline level. Combing the pristine baseline (without target miR-122) and signal amplification by TCEP, we demonstrated the detection of miR-122 within minutes at an extremely low level with a wide detection range from 0.1 fM to 0.5 nM. The amplified current signal enabled one-step detection by CV at microelectrode sensors previously inaccessible. Combined diagnosis power in CV and great sensitivity in SWV are highly advantageous in the method development and parameter optimization. Moreover, quantification of the absolute miRNA abundance is achieved via direct electrochemical readout that is significant for biomedical research and offers promising potentials in clinical and in-home POC applications. The sensor exhibited superior mismatch discrimination capability owing to the three-stem double helix design that has been validated in macroscopic electrochemical DNA sensors. The excellent stability and reproducible surface regeneration with GHCl further enables systematic and quantitative analysis. The sensor design is generalizable for other miRNA sequences. Ongoing study of the kinetic mechnism could further expand the dynamic range and lower the limit of detection. Given the fact that the sensor was developed on a small-scale electrode, the established sensor platform is believed to be a promising high-throughput diagnostic tool, either for point-of-care monitoring of the pre-established miRNA siganatures as disease biomarkers or, in the long-term, for the determination of miRNA signatures to compliment the existing techniques such as qRT-PCR but offer direct quantification.

ASSOCIATED CONTENT

Supporting Information

The Supporting Information is available free of charge on the ACS Publications website at DOI: 10.1021/acs.analchem.5b00780.

Microelectrode and sensor characterizations; CV and SWV responses in different microRNA concentrations and TCEP concentrations; frequency depencence; current analysis; mismatch discrimination (PDF)

AUTHOR INFORMATION

Corresponding Authors

*E-mail: dmerlin@gsu.edu. Tel: (404) 413-3592.
*E-mail: glwang@gsu.edu. Tel: (404) 413-5507.

Notes

The authors declare no competing financial interest.

ACKNOWLEDGMENTS

This work was supported by grants from the Department of Veterans Affairs (Merit Award: BX002526 to D.M.) and the National Institutes of Health of Diabetes and Digestive and Kidney by the Grants RO1-DK-071594 and RO1-DK-064711 (to D.M.). Dr. Viennois is the recipient of a Research Fellowship award from the Crohn's & Colitics Foudation of America. Dr. Merlin is a recipient of a Career Scientist Award from the Department of Veterans Affairs.

REFERENCES

(1) Dong, H.; Lei, J.; Ding, L.; Wen, Y.; Ju, H.; Zhang, X. *Chem. Rev.* **2013**, *113*, 6207.
(2) Lewis, B. P.; Burge, C. B.; Bartel, D. P. *Cell* **2005**, *120*, 15.
(3) Cullen, B. R. *Nature* **2009**, *457*, 421.
(4) Laterza, O. F.; Lim, L.; Garrett-Engele, P. W.; Vlasakova, K.; Muniappa, N.; Tanaka, W. K.; Johnson, J. M.; Sina, J. F.; Fare, T. L.; Sistare, F. D.; Glaab, W. E. *Clin. Chem.* **2009**, *55*, 1977.
(5) Wang, K.; Zhang, S.; Marzolf, B.; Troisch, P.; Brightman, A.; Hu, Z. *Proc. Natl. Acad. Sci. U. S. A.* **2009**, *106*, 4402.
(6) Chen, X.; Ba, Y.; Ma, L.; Ma, L. J.; Cai, X.; Yin, Y.; Wang, J. H.; Guo, J. G.; Zhang, Y. J.; Chen, J. N.; Guo, X.; Li, Q. B.; Li, X. Y.; Wang, W. J.; Zhang, Y.; Wang, J.; Jiang, X. Y.; Xiang, Y.; Xu, C.; Zheng, P. P.; Zhang, J. B.; Li, R. Q.; Zhang, H. J.; Shang, X. B.; Gong, T.; Ning, G.; Wang, J.; Zen, K.; Zhang, J. F.; Zhang, C. Y. *Cell Res.* **2008**, *18*, 997.
(7) Kosaka, N.; Iguchi, H.; Ochiya, T. *Cancer Sci.* **2010**, *101*, 2087.
(8) Michel, V.; Yuan, Z.; Ramsubir, S.; Bakovic, M. *Exp. Biol. Med.* **2006**, *231*, 490.

DOI: 10.1021/acs.analchem.5b00780
Anal. Chem. 2015, 87, 8173−8180

(9) Klein, D. *Trends Mol. Med.* **2002**, *8*, 257.
(10) Lim, L. P. *Genes Dev.* **2003**, *17*, 991.
(11) Liang, Y.; Ridzon, D.; Wong, L.; Chen, C. *BMC Genomics* **2007**, *8*, 166.
(12) Lautner, G.; Gyurcsányi, R. E. *Electroanalysis* **2014**, *26*, 1224.
(13) Lee, J. M.; Jung, Y. *Angew. Chem., Int. Ed.* **2011**, *50*, 12487.
(14) Liu, C. G.; Calin, G. A.; Meloon, B.; Gamliel, N.; Sevignani, C.; Ferracin, M.; Dumitru, C. D.; Shimizu, M.; Zupo, S.; Dono, M.; Alder, H.; Bullrich, F.; Negrini, M.; Croce, C. M. *Proc. Natl. Acad. Sci. U. S. A.* **2004**, *101*, 9740.
(15) Thomson, J. M.; Parker, J.; Perou, C. M.; Hammond, S. M. *Nat. Methods* **2004**, *1*, 47.
(16) Lodes, M. J.; Caraballo, M.; Suciu, D.; Munro, S.; Kumar, A.; Anderson, B. *PLoS One* **2009**, *4*, e6229.
(17) Asaga, S.; Kuo, C.; Nguyen, T.; Terpenning, M.; Giuliano, A. E.; Hoon, D. S. B. *Clin. Chem.* **2011**, *57*, 84.
(18) Zhi, F.; Cao, X.; Xie, X.; Wang, B.; Dong, W.; Gu, W.; Ling, Y.; Wang, R.; Yang, Y.; Liu, Y. *PLoS One* **2013**, *8*, e56718.
(19) Gaur, A.; Jewell, D. A.; Liang, Y.; Ridzon, D.; Moore, J. H.; Chen, C.; Ambros, V. R.; Israel, M. A. *Cancer Res.* **2007**, *67*, 2456.
(20) Zhang, J.; Li, Z.; Wang, H.; Wang, Y.; Jia, H.; Yan, J. *Chem. Commun.* **2011**, *47*, 9465.
(21) Gao, Z. Q.; Yu, Y. H. *Biosens. Bioelectron.* **2007**, *22*, 933.
(22) Gao, Z. Q.; Yu, Y. H. *Sens. Actuators, B* **2007**, *121*, 552.
(23) Gao, Z. Q.; Peng, Y. F. *Biosens. Bioelectron.* **2011**, *26*, 3768.
(24) Gao, Z. Q. *Analyst* **2012**, *137*, 1674.
(25) Labib, M.; Khan, N.; Ghobadloo, S. M.; Cheng, J.; Pezacki, J. P.; Berezovski, M. V. *J. Am. Chem. Soc.* **2013**, *135*, 3027.
(26) Labib, M.; Ghobadloo, S. M.; Khan, N.; Kolpashchikov, D. M.; Berezovski, M. V. *Anal. Chem.* **2013**, *85*, 9422.
(27) Labib, M.; Khan, N.; Berezovski, M. V. *Anal. Chem.* **2015**, *87*, 1395.
(28) Wang, J. X.; Yi, X. Y.; Tang, H. L.; Han, H. X.; Wu, M. H.; Zhou, F. M. *Anal. Chem.* **2012**, *84*, 6400.
(29) Pohlmann, C.; Sprinzl, M. *Anal. Chem.* **2010**, *82*, 4434.
(30) Hu, J.; Wang, T.; Kim, J.; Shannon, C.; Easley, C. J. *J. Am. Chem. Soc.* **2012**, *134*, 7066.
(31) Salamifar, S. E.; Lai, R. Y. *Anal. Chem.* **2014**, *86*, 2849.
(32) Liu, J.; Wagan, S.; Davila-Morris, M.; Taylor, J.; White, R. J. *Anal. Chem.* **2014**, *86*, 11417.
(33) Bard, A. J.; Faulkner, L. R. *Electrochemical Methods: Fundamentals and Applications*, 2nd ed.; Wiley: New York, 1980.
(34) Zhang, B.; Galusha, J.; Shiozawa, P. G.; Wang, G. L.; Bergren, A. J.; Jones, R. M.; White, R. J.; Ervin, E. N.; Cauley, C. C.; White, H. S. *Anal. Chem.* **2007**, *79*, 4778.
(35) Sassolas, A.; Leca-Bouvier, B. D.; Blum, L. J. *Chem. Rev.* **2008**, *108*, 109.
(36) Zhang, Y.; Jia, Y.; Zheng, R.; Guo, Y.; Wang, Y.; Guo, H.; Fei, M.; Sun, S. *Clin. Chem.* **2010**, *56*, 1830.
(37) Starkey Lewis, P. J.; Dear, J.; Platt, V.; Simpson, K. J.; Craig, D. G.; Antoine, D. J.; French, N. S.; Dhaun, N.; Webb, D. J.; Costello, E. M.; Neoptolemos, J. P.; Moggs, J.; Goldring, C. E.; Park, B. K. *Hepatology* **2011**, *54*, 1767.
(38) Coulouarn, C.; Factor, V. M.; Andersen, J. B.; Durkin, M. E.; Thorgeirsson, S. S. *Oncogene* **2009**, *28*, 3526.
(39) Xiao, Y.; Lou, X.; Uzawa, T.; Plakos, K. J. I.; Plaxco, K. W.; Soh, H. T. *J. Am. Chem. Soc.* **2009**, *131*, 15311.
(40) Flynn, N. T.; Tran, T. N. T.; Cima, M. J.; Langer, R. *Langmuir* **2003**, *19*, 10909.
(41) Furst, A. L.; Hill, M. G.; Barton, J. K. *Polyhedron* **2014**, *84*, 150.
(42) Lapierre-Devlin, M. A.; Asher, C. L.; Taft, B. J.; Gasparac, R.; Roberts, M. A.; Kelley, S. O. *Nano Lett.* **2005**, *5*, 1051.
(43) Fang, Z. C.; Kelley, S. O. *Anal. Chem.* **2009**, *81*, 612.
(44) Kang, D.; Zuo, X.; Yang, R.; Xia, F.; Plaxco, K. W.; White, R. J. *Anal. Chem.* **2009**, *81*, 9109.
(45) Ferapontova, E. E.; Olsen, E. M.; Gothelf, K. V. *J. Am. Chem. Soc.* **2008**, *130*, 4256.
(46) Liu, J.; Wang, D.; Kvetny, M.; Brown, W.; Li, Y.; Wang, G. *Anal. Chem.* **2012**, *84*, 6926.
(47) Liu, J.; Kvetny, M.; Feng, J.; Wang, D.; Wu, B.; Brown, W.; Wang, G. *Langmuir* **2012**, *28*, 1588.
(48) Feng, J.; Liu, J.; Wu, B.; Wang, G. *Anal. Chem.* **2010**, *82*, 4520.
(49) White, R. J.; Plaxco, K. W. *Anal. Chem.* **2010**, *82*, 73.
(50) Srisombat, L.; Park, J.-S.; Zhang, S.; Lee, T. R. *Langmuir* **2008**, *24*, 7750.

DOI: 10.1021/acs.analchem.5b00780
Anal. Chem. 2015, 87, 8173−8180